Eur. Phys. J. E (2021) 44:93, https://doi.org/10.1140/epje/s10189-021-00096-9

A mechanical test of the tenertaxis hypothesis for leukocyte diapedesis

S.M. Amin Arefi[1], Cheng Wei Tony Yang[2], Don D. Sin[2] and James J. Feng[1,3*]

[1] Department of Chemical and Biological Engineering, University of British Columbia, Vancouver, BC V6T 1Z3, Canada

[2] Centre for Heart Lung Innovation, St Paul's Hospital and University of British Columbia, Vancouver, BC V5Z 1M9, Canada

[3] Department of Mathematics, University of British Columbia, Vancouver, BC V6T 1Z2, Canada

(July 9, 2021)

Abstract

As part of the immune response, leukocytes can directly transmigrate through the body of endothelial cells or through the gap between adjacent endothelial cells. These are known, respectively, as the transcellular and paracellular route of diapedesis. What determines the usage of one route over the other is unclear. A recently proposed tenertaxis hypothesis claims that leukocytes choose the path with less mechanical resistance against leukocyte protrusions. We examined this hypothesis using numerical simulation of the mechanical resistance during paracellular and transcellular protrusions. By using parameters based on human lung endothelium, our results show that the required force to breach the endothelium through the transcellular route is greater than paracellular route, in agreement with experiments. Moreover, experiments have demonstrated that manipulation of the relative strength between the two routes can make the transcellular route preferable. Our simulations have demonstrated this reversal, and thus tentatively confirmed the hypothesis of tenertaxis.

*Corresponding author. E-mail: james.feng@ubc.ca

1 Introduction

The immune response requires recruitment of leukocytes to defend the body against foreign microorganisms such as bacteria and viruses. The leukocytes first form weak adhesion and roll on the endothelium surface. Then they bind firmly on the endothelial surface, pass through the endothelium in a process called diapedesis, and breach the basement membrane. Finally, they move toward the chemotactic stimulus in the tissue [1]. Thus, reaction to infections requires frequent crossing of leukocytes through the layer of endothelial cells (ECs). To initiate the transmigration, leukocytes extend invadosome-like protrusions (ILPs) into the endothelium [2]. They can transmigrate either directly through the body of an individual EC (the transcellular route) or through the junction between ECs (the paracellular route) [2]. It is unclear what determines the path of transmigration.

To address this question, Martinelli *et al.* [3] conducted three *in vitro* tests to examine the correlation between junctional integrity and the route of diapedesis. First, they compared the diapedesis through rat brain and heart and human heart and lung endothelia. The rat brain endothelium has stronger junctional integrity than heart and lung endothelia. They observed that for the rat brain endothelium the number of transcellular diapedesis is higher than the paracellular diapedesis, while in rat heart and also human heart and lung endothelia, the usage of paracellular route is dominant. Second, they used drugs and hormones to enhance or disrupt endothelial junctions in rat brain and heart tissues. They noticed that disrupting junctional integrity leads to a remarkable increase (about two folds) in paracellular diapedesis accompanied by decrease in transcellular transmigration. Finally, they exposed human lung endothelium to long-term shear flow as a mechanical modifying agent to promote the junctional strength and remodeling of the cytoskeleton. This alteration causes a significant increase in transcellular diapedesis. Based on these observations, Martinelli *et al.* [3] concluded that strong junctional integrity is correlated with dominant transcellular route of transmigration, and the EC junction tightness and local stiffness are the major determinants of the route of diapedesis. They hypothesized that leukocytes choose a path with the least mechanical resistance during transmigration, a tendency termed tenertaxis [3,4].

Conceptually, the hypothesis appears plausible. But from a physical viewpoint, it raises several interesting questions. For example, as the leukocyte extends ILPs into the EC, how much resistance can the EC generate in either the transcellular and paracellular route? Given the typical level of

protrusion forces in the ILPs, will they be able to overcome the resistance to effect a transmigration through either route? Will the difference in resistance correspond with experimental observations of the prevalence of one route over the other, under wild-type conditions and active intervention?

In this study, we test the tenertaxis hypothesis quantitatively by using a computational model of the endothelium and leukocytes with ILPs. To answer the questions raised above, we perform two subtasks. First, we review existing data on the mechanical properties of ECs in different tissues in their physiologic or altered states, as well as data on the shape and size of the invadosomes and representative magnitudes of the protrusive forces inside them. Thus we identify a reasonable range of the mechanical parameters corresponding with prior experimental observations. Second, we use continuum theories of hyperelasticity and contact mechanics to simulate the penetration of an ILP through an EC body (transcellular) and through an EC-EC junction (paracellular). Our model predicts lower resistance in one route or the other depending on the endothelial properties in its natural or altered state. These outcomes are consistent with experimental observations of the prevalence of trans- or paracellular diapedesis. Thus, the model tentatively confirms the tenertaxis hypothesis.

2 Problem setup and methodology

According to the tenertaxis hypothesis, leukocytes extend ILPs into the EC to seek the route of least resistance [4]. Essentially, this amounts to comparing the mechanical resistance of the two potential routes: one against the formation of a tunnel through the EC body and the other against a protrusion through the endothelial junctional opening. Therefore, our model is centered on computing the mechanical resistance of the ECs monolayer against the protrusive force of the leukocytes in either route. As such, the model needs to represent at least the following three components (Fig. 1):

(a) The ILP. We model the leukocyte protrusion as a nearly rigid rod with a diameter of 340 nm based on the average of protrusions observed in experiments [2, 4]. To simulate the rod penetrating the EC cell body or the EC junction, we can either specify the force on the rod or prescribe its displacement. Most of the results will be presented according to the latter protocol for simplicity and convenience.

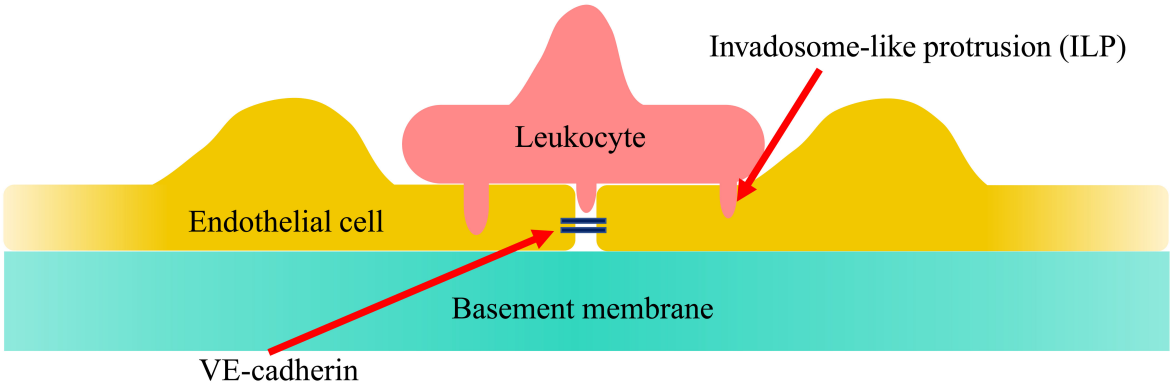

Figure 1: Schematic of a leukocyte extending invadosome-like protrusions (ILPs) on the endothelium into the EC cell body and through the EC cell junction. The latter consists of transmembrane adhesive proteins (e.g. VE-cadherins) bridging a gap between the two ECs.

(b) The ECs and the basement membrane underneath. We treat the ECs and the basement membrane as hyperelastic solid components obeying the neo-Hookean constitutive equation, ignoring the cytosol and other organelles inside the cell [5]. The EC nucleus is very stiff and diapedesis rarely happens in the area around the nucleus [4]. Therefore, we do not consider penetrations through the nuclear bulge of Fig. 1.

(c) Endothelial cell-cell junctions. We model the EC junction as a preexisting narrow gap between two neighboring ECs, with an undeformed gap size of 10 nm [6, 7]. The gap is bridged by bonds that consist of transmembrane adhesive proteins such as vascular endothelial cadherins (VE-cadherins) [8]. We model the molecular bonds as linear springs distributed between two adjacent EC edges [9, 10].

2.1 Geometric setup

Figure 2 shows the two geometries used for simulating the penetration of an ILP through the EC junction (Fig. 2*a*) and through the body of an EC (Fig. 2*b*). Because the diameter of the ILP is only about 2% that of the EC [4, 11], the penetration is largely a local event that does not involve the entire EC body. Thus, we circumscribe a small portion or subdomain of the endothelium for the simulations to reduce the computational cost. The subdomain used for the modeling of the paracellular protrusion is a three-dimensional cylinder 3 μm in diameter and includes two adjacent ECs, the junction and the basement membrane underneath (Fig. 2*a*). The undeformed heights of

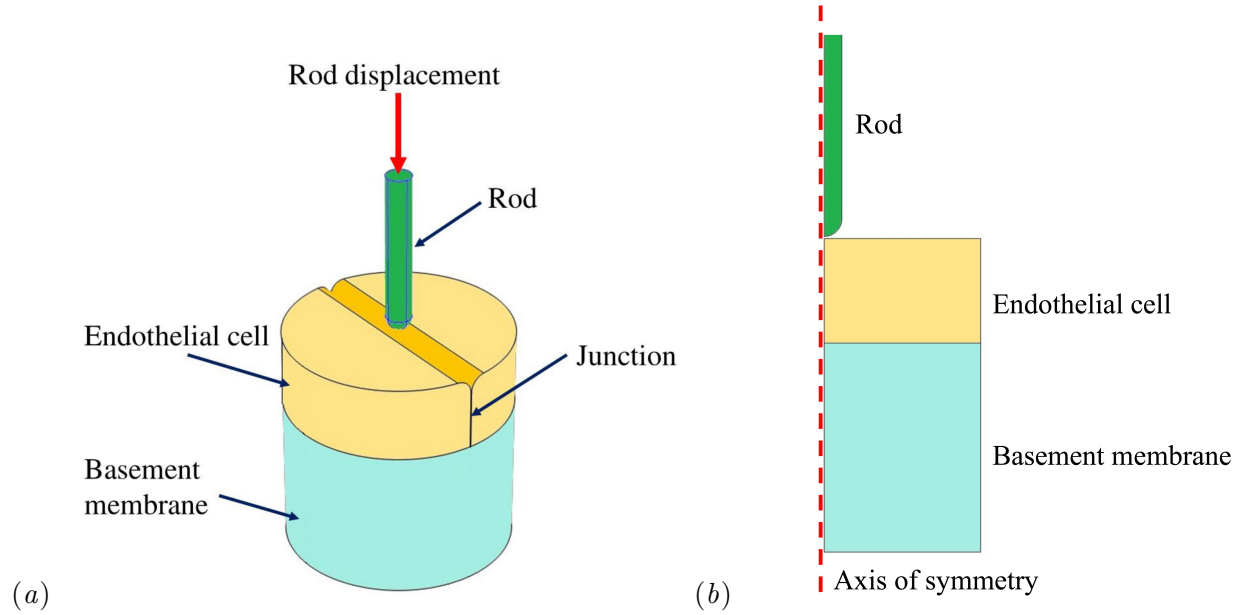

Figure 2: Geometric setup for the simulations of (a) the paracellular protrusion, and (b) the transcellular protrusion. Initially, the tip of the rod is 10 nm above the flat apical surface of the endothelium in (a) and 20 nm in (b).

the EC and the basement membrane are respectively 1 μm and 2 μm [12, 13]. The junctional gap has an undeformed width of $d_{gap} = 10$ nm [6, 7]. Its top opens into a groove, with two opposed circular arcs of radius 200 nm subtending a central angle of 90°. For the transcellular protrusion, we use a two-dimensional axisymmetric domain 1.5 μm in radius that comprises a part of the EC body (undeformed height of 1 μm, away from the nucleus and the junction) and the basement membrane underneath (undeformed height of 2 μm) (Fig. 2b). The protrusion is modeled as a rod 340 nm in diameter [4], with a cylindrical body and a hemispherical head.

To simulate the penetration process, we prescribe the kinematics of the movement of the ILP into the EC in terms of its tip displacement $d_{rod}(t)$. As the EC deforms, the contact force on the ILP is computed by integrating the traction over the ILP surface in contact with the EC. This yields the resistance force on the ILP, $F_r(d_{rod})$, as a function of the depth d_{rod}. Because the elastic deformation happens instantaneously, without viscous damping, essentially we are computing a series of quasi-static states with the rod at different positions of insertion. Thus, the speed of motion $d'_{rod}(t)$ plays no role in the result. In addition, we have carried out dynamic simulations by specifying a constant pushing force on the ILP and tracking its movement in time. The two protocols essential confirm each other, and we will mostly present data on the quasi-static $F_r(d_{rod})$

for simplicity.

The simulation ends when the displacement d_{rod} reaches a threshold d_b for breakthrough. This threshold is set to the thickness of the EC monolayer (d_b =1 μm) for the paracellular protrusion and $d_b = 0.98$ μm for the transcellular protrusion. The threshold of 0.98 μm for the transcellular protrusion was chosen because the thickness of the EC membrane is 10 nm [14,15], and at this point the apical membrane reaches the basal membrane so they may open up a transcellular tunnel [4]. After breakthrough, the leukocyte tends to spread between the EC and the basement membrane *in vivo* [16] or a substrate *in vitro* [3, 4], and we will not model that spread.

2.2 Governing equations and numerics

We treat the ECs and the basement membrane as neo-Hookean hyperelastic materials that can capture the strain-stiffening behaviour of biological materials [17], both obeying the following constitutive equation with different material properties:

$$\boldsymbol{\sigma} = G\, J^{-\frac{5}{3}} \left(\boldsymbol{F}\boldsymbol{F}^T - \frac{\boldsymbol{I}}{3} \operatorname{tr}\big(\boldsymbol{F}\boldsymbol{F}^T\big) \right) - K(J-1)\boldsymbol{I}, \tag{1}$$

where $F_{ij} = \partial x_i / \partial X_j$ is the deformation gradient tensor, with $\boldsymbol{X}$ and $\boldsymbol{x}$ being the undeformed and current positions of a material point, and $J = \det\{\boldsymbol{F}\}$. The coefficients G and K are the shear and bulk modulus, respectively, connected via the Poisson ratio ν: $K = \frac{2G}{3}\frac{1+\nu}{1-2\nu}$. Finally, the governing equation of solid deformation is given by:

$$\nabla \cdot \boldsymbol{\sigma} = 0. \tag{2}$$

In terms of boundary conditions, the basal surface of the basement membrane has zero displacement, while all the other surfaces are free to deform with no load or constraint (Fig. 2). In the paracellular geometry of Fig. 2a, we deploy distributed elastic springs between the opposite lateral surfaces of the two adjacent ECs to model the cell-cell adhesion force because of VE-cadherin bonds. Details of the junction model will be given below.

We use the augmented Lagrange method and the penalty method to model the normal contact force between the rod and the EC surface during transcellular and paracellular penetration, respec-

tively [18]. Also we assume a frictionless contact between the protrusion and the ECs [19]. The sets of equations were solved using COMSOL Multiphysics. A special numerical challenge is to capture the very large strain under the ILP in the transcellular setup, and we meet it by employing a very high aspect-ratio rectangular mesh in the surrounding area with quintic Lagrange shape function for the elements. Details can be found in the online Supplemental Information (SI).

2.3 Parameter estimation

To test the tenertaxis hypothesis, a prerequisite is to estimate the mechanical rigidity of the EC body as well as the EC junctions. These bear directly on the resistance against transmigration through the transcellular and paracellular routes, and hence the preference for one route or the other. In the following we estimate the elastic modulus of the human lung microvascular endothelial cells and the mechanical properties of their junction. The outcome of this exercise is the baseline values summarized in Table 1 for some key mechanical parameters.

Symbol	**Description**	**Value**	**Sources**
E_{para}	Elastic modulus of EC body for paracellular route	1800 Pa	[20]
E_{tran}	Elastic modulus of EC body for transcellular route	180 Pa	[20, 21]
E_{BM}	Elastic modulus of the basement membrane	5000 Pa	[17]
ν	Poisson's ratio	0.3	[17]
L_0	Rest length of junctional bonds	10 nm	[10]
k_b	Spring constant of junctional bonds	2×10^{-5} N/m	[9]
N_b	Areal density of junctional bonds	20 μm^{-2}	[22, 23]

Table 1: Baseline values for key parameters used in our model, estimated for human lung microvascular endothelial cells.

2.3.1 Endothelial cells

The elastic modulus of ECs has most often been measured from the response of the cells to indentation, e.g., by the tip of an atomic force microscope (AFM) [24]. Generally, the elastic modulus tends to be higher above the nucleus and lower toward the periphery. For different types of human tissues, the EC body modulus, away from the nucleus, falls in the range $E = 1000 \sim 5800$ Pa [17, 20, 24–27]. For example, Viswanathan *et al.* [20] reported $E = 1800$ Pa near the periphery of human lung microvascular endothelial cells (HLMVECs). For human umbilical vein endothelial cells (HUVECs), E varies from 6800 Pa on the top of the nucleus to 1400 Pa near the cell edge [25]. For human aortic endothelial cells (HAECs), $E = 5800$ Pa is recorded above stress fibers while

$E = 1500$ Pa away from stress fibers [27]. To propose the tenertaxis hypothesis, Martinelli *et al.* [3] quoted data on HLMVECs among other types of ECs. Accordingly, we adopt the HLMVEC cell-body modulus [20] for simulating the paracellular protrusion: $E_{para} = 1800$ Pa. This value is also close to the modulus of the cell body of HUVECs and HAECs.

To estimate the EC modulus during transcellular diapedesis, a complication arises from the fact that a leukocyte, upon adhering to the apical surface of an EC, *actively remodels* the EC cortex underneath [21, 28]. Thus, the effective EC modulus is much reduced in comparison to areas away from the leukocyte attachment site. After removing an attached leukocyte by nano-surgery, Isac *et al.* [21] observed depolymerization of F-actin and remodeling of the EC cytoskeleton underneath the site of attachment. Barzilai *et al.* [28] showed similar disassembly of actin filaments underneath a leukocyte protrusion. Furthermore, Isac *et al.* [21] measured the EC elastic modulus at the attachment site using AFM indentation. The site can be up to 10 times softer than its surrounding area, with E dropping from ~ 3000 Pa to ~ 300 Pa for HUVECs. This trend is consistent with the observation that indenting HAECs above stress fibers would yield a much stiffer modulus than away from stress fibers [27]. Unfortunately, we have found no quantitative data on the softening of HLMVEC modulus. Since we wish to model the HLMVEC-based experiments of Martinelli *et al.* [3], we borrow the softening factor of 10 from the HUVEC data [21]. Based on the modulus of 1800 Pa for the intact HLMVEC, we adopt an effective $E_{tran} = 180$ Pa for the transcellular simulation.

For both paracellular and transcellular simulations, the elastic modulus of the basement membrane is taken to be $E_{BM} = 5000$ Pa, similar to the elastic modulus of extracellular matrix [17].

2.3.2 Endothelial junctions

The EC junction consists of a narrow gap bridged by molecular bonds (Fig. 1). As an ILP penetrates through the gap, it widens the gap by separating the EC surfaces and stretching the bonds. Following earlier studies, we represent the bonds by linear elastic springs [9, 10, 14], with the following elastic force on each bond:

$$f_b = k_b(L_b - L_0), \tag{3}$$

where k_b is the spring constant, L_b is the bond length and L_0 is the equilibrium bond length. The spring constant k_b was reported to be $k_b = 10^{-5} \sim 10^{-2}$ N/m for cell-cell adhesion bonds [9], and the equilibrium bond length $L_0 = 10 \sim 20$ nm [6, 10]. We have taken $k_b = 2 \times 10^{-5}$ N/m and L_0 =10 nm to be our baseline values, the latter being consistent with the undeformed gap width at the junction.

The areal bond density N_b has been modeled by a kinetic equation for the formation and dissociation of bonds, with the rate constants being functions of tension in the bonds [10, 14]. For simplicity, we ignore the kinetics of N_b and adopt a constant equilibrium value based on prior observations. The total number of bonds between two ECs falls in a wide range, and the areal density of bonds can be estimated as $N_b = 5 \sim 50000$ μm^{-2} [6, 9, 10]. Furthermore, from the measured normal stress ($\sim$ 1 nN/μm^2) at the junction [22] and the maximum force ($\sim$ 50 pN) that each bond can sustain [23], one can estimate $N_b = 20$ μm^{-2}. This is the value that we have adopted.

In our finite-element simulation, the bond force is applied to each mesh point on the portion of the EC surface that forms the junction. Each mesh point is assigned an associated surface area A_i based on the mesh configuration. The bond length L_b at the mesh point is the horizontal distance to the opposite cell face. Thus, we calculate a horizontal bond force $F_i = A_i N_b k_b (L_b - L_0)$, and apply it onto the mesh point.

For the parameters estimated above, the junctional springs turn out to contribute a small amount of the resistance to paracellular diapedesis; most of the resistance comes from the deformation of the EC cells. This is because the bond forces are horizontal, and only contribute indirectly to the resistance by affecting the EC surface shape. In particular, its contribution vanishes toward the end, when the junctional gap becomes widened more or less uniformly to the size of the rod. The minor role of the junctional springs alleviates the concern about uncertainties in estimating the above parameters.

We have carried out a parametric study to examine how the model predictions vary with the key geometric and mechanical parameters. Details are given in the online SI.

3 Results and discussion

We focus on the resistance force on the ILP as it extends across the endothelium through the transcellular or paracellular route. This resistance force is used to predict which is the preferred route with the smaller resistance. We first present results using the baseline parameters corresponding to wild-type HLMVECs, and then investigate the effects of manipulating the elastic modulus of the endothelium.

3.1 Transmigration predicted using the baseline parameters

3.1.1 Paracellular route

In our quasi-static protocol, we move the rod representing the ILP downward into the junctional gap by 10 nm each time, and compute the resistance force F_r on it from the contact surfaces between the rod and the two neighboring ECs. Figure 3(a) plots the force as a function of the displacement of the tip of the rod d_{rod}. Because of the geometry of the problem, the rod travels downward by about 75 nm before it makes contact with the EC surfaces at the top of the junctional gap. Initially, the rod deforms the upper edges of the ECs at the junction and opens it up into a wedge. The resistance force F_r rises sharply as a result. It peaks at 35 pN, for $d_{rod} \approx 0.25$ μm, when the rod pushes the edges of the ECs apart so that the tip of the wedge reaches the basal EC surface (Fig. 3b). As the rod pushes further down, it opens an increasingly larger portion of the junction into a cylindrical hole, which does not provide much upward resistance. Therefore, F_r starts to decline with d_{rod}. This suggests a discontinuous jump in a dynamic simulation, and we will return to this point later. The minimum resistance $F_r = 20.3$ pN occurs at $d_{rod} \approx 0.54$ μm (Fig. 3c). Afterwards, the basal face of the EC starts to cause appreciable deformation in the basement membrane, which is much stiffer than the EC (Table 1). Thus, F_r starts to increase again with displacement. This increase continues till the end of the penetration, when the rod reaches the basement membrane ($d_{rod} = d_b = 1$ μm). Thus, the maximum resistance force $F_{max} = 45$ pN occurs at the end of the paracellular transmigration. The process is illustrated in Movie 1 in the SI.

Is it reasonable to expect the ILP to produce a protrusive force large enough to overcome such a resistance? Earlier studies showed that the protrusive force is mainly due to actin filaments

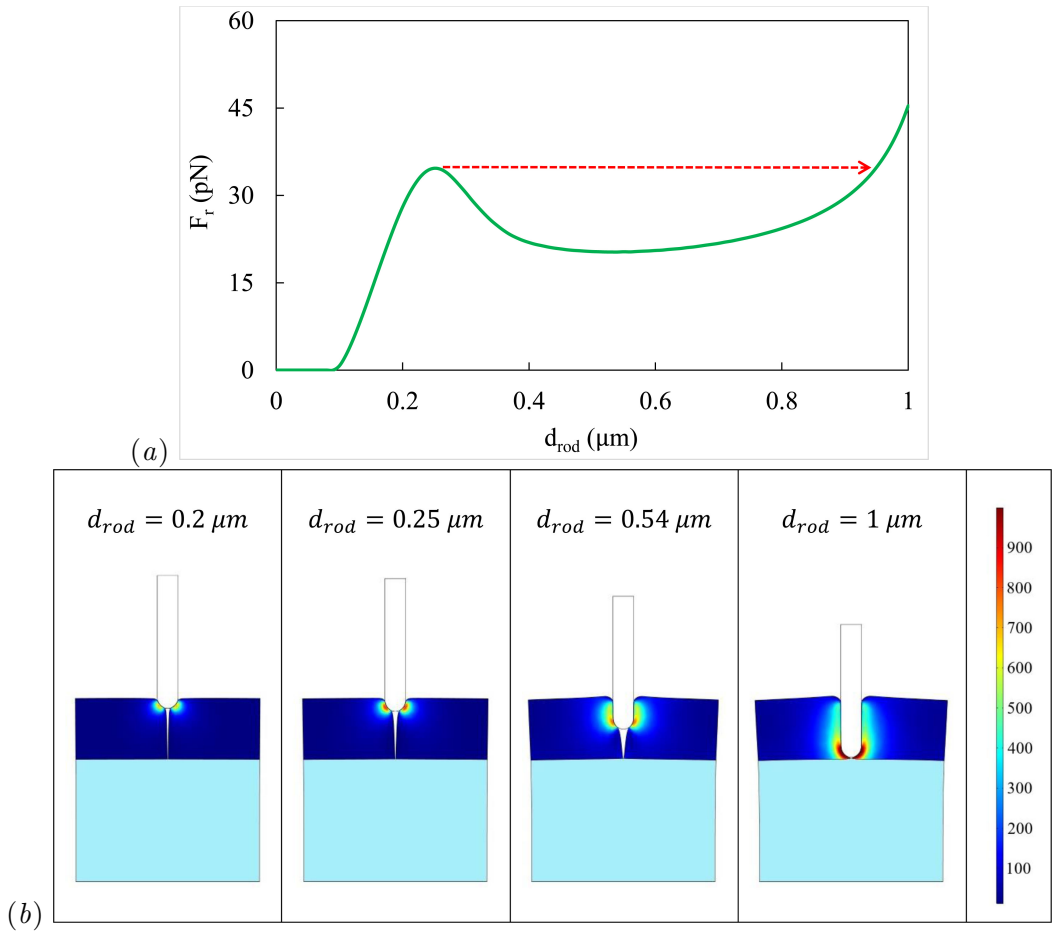

Figure 3: (a) The vertical contact force as a function of the rod displacement during paracellular protrusion. The dashed arrow suggests how the rod will pass over an unstable portion of the curve in a dynamic simulation with a prescribed force. Penetration occurs when d_{rod} reaches the breakthrough threshold $d_b = 1$ μm. (b) Cross-sectional view of the mid-plane normal to the groove atop the EC junction (see Fig. 2a) at several points of the transmigration, with contours of the von Mises stress in Pa. The ECs and the basement membrane are colored dark blue and light blue, respectively.

polymerizing in the core of the ILP, with little direct contribution from myosin [29]. The force generated by a single polymerizing actin filament ranges between 1.3 and 9 pN [30, 31]. Each protrusion may contain between 10 and 30 actin filaments [32]. Thus, the ILP can easily generate a protrusive force that matches the resistance of the paracellular route.

Because of the quasi-static setup of the problem, in which we prescribe the displacement of the rod, the force-displacement curve of Fig. 3(a) has interesting implications for a "dynamic simulation" where we prescribe the pushing force F_r on the rod, and compute its displacement $d_{rod}(t)$. If F_r is below 35 pN, the rod will stop on the first up-slope of the curve in Fig. 3(a). With

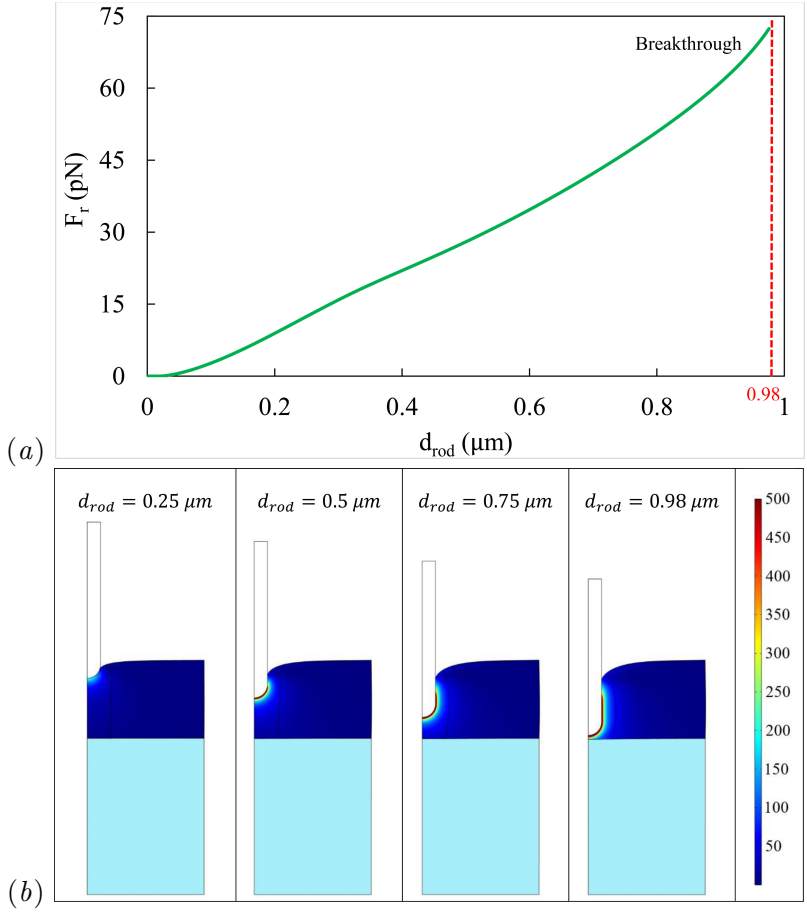

Figure 4: (a) The vertical contact force as a function of the rod displacement during transcellular protrusion. The vertical dashed line marks the breakthrough threshold $d_b = 0.98$ μm. (b) The meridian plane of the axisymmetric geometry (see Fig. 2b) at several points of the transmigration, with contours of the von Mises stress in Pa. The ECs and the basement membrane are colored dark blue and light blue, respectively.

larger forces, the rod passes the peak, and then jumps over an unstable portion of the curve to land on a larger displacement on the second up-slope of the curve. This is indicated by the red dashed arrow in Fig. 3(a). In fact, we have done such dynamic simulations to confirm the above scenarios. Details are discussed in the SI, with a simulation shown in Movie 2. Of course, there would be a jump in the opposite direction if we start with an initial state of full penetration and then gradually decrease the protrusion force. But such a scenario is not relevant to the diapedesis process.

3.1.2 Transcellular route

To test transcellular protrusion, we again adopt a quasi-static approach by moving the ILP downward by small increments and compute the elastic resistance by the EC. Figure 4(a) plots the vertical contact force during the progression of the rod, while Fig. 4(b) depicts the contours of the von Mises stress on the meridian plane at several points of the transcellular penetration of the EC. The protrusive force on the EC produces a transcellular tunnel similar to the finger-like protrusions of leukocytes observed in the experiments [3, 4]. The force F_r increases monotonically but non-linearly with the depth of penetration d_{rod}, owing to the geometric non-linearity of the deformation and the hyperelastic behaviour of the EC. Thus, when the protrusion reaches the threshold of $d_b = 0.98$ μm, the resistance force attains its maximum during the transcellular penetration: $F_{max} = 72$ pN.

Prior experiments show that paracellular transmigration is the preferred mode for HLMVECs [3, 4] and HUVECs [33]. Across an HLMVEC monolayer, for example, paracellular diapedesis occurs about 65% of the time *in vitro* [3, 4]. Based on baseline parameters corresponding to HLMVECs, our model predicts a maximum mechanical resistance of 45 pN and 72 pN in the paracellular and trancellular routes, respectively. This shows that the penetration is easier using the paracellular route, in agreement with experimental observations [3, 4]. To probe the tenertaxis hypothesis further, however, we need to manipulate the relative level of resistance in the EC body and junctional areas. This was achieved in prior experiments by drug or hormone treatment, shear flow effect, and comparing different cell types that offer different levels of junctional resistance. In the following, we will simulate such changes by manipulating the endothelial resistances at the cell junctions.

3.2 Effect of manipulating endothelial stiffness at the junction

In a series of experiments, Martinelli *et al.* [3, 4, 34] demonstrated two interesting trends. First, for HLMVECs in their natural physiologic state, the paracellular route is preferred and accounts for 65% of the total transmigration events. Second, by strengthening the EC stiffness near junctions, a reversal in this preference can be achieved, with a majority (70%) of the transmigration occurring through the transcellular route. This has motivated us to manipulate the junctional strength in

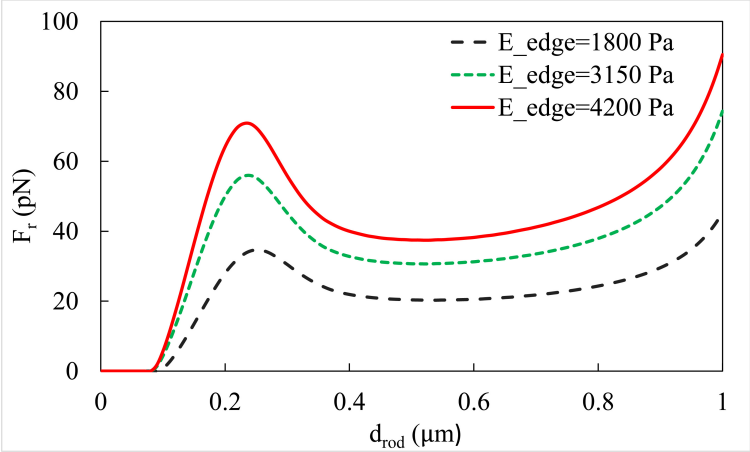

Figure 5: Effect of raising the EC modulus near the cell edges on the resistance force during paracellular penetration. The baseline value is $E_{para} = 1800$ Pa (see Table 1), and the two higher values correspond to experimental manipulations of EC edge rigidity [3, 20].

our model to see how that modifies the relative resistance of the two routes.

Using the hormone adrenomedullin, Martinelli *et al.* [3] managed to increase the level of cortical F-actin near the HLMVEC edges. As a result, the EC elastic modulus rose to 1.75 times of its baseline value. Moreover, Viswanathan *et al.* [20] reported increase of HLMVEC modulus by a factor of 2.33 after treatment with hepatocyte growth factor. Away from the cell edge, the EC body modulus is not affected by the chemical treatment, and neither is the transcellular migration [3, 20, 35, 36]. In view of these experimental data, we will increase E_{para} by a factor of 1.75 and 2.33 from its baseline value of 1800 Pa, to $E_{para} = 3150$ Pa and 4200 Pa, respectively. None of the experiments indicated modifications of the VE-Cadherin-based molecular bonds at the EC junctions. Thus, we have kept the baseline values of $k_b = 2 \times 10^{-5}$ N/m.

Figure 5 depicts the effect of stiffer EC-edge modulus on the resistance force during ILP penetration. The maximum resistance force F_{max} has increased markedly for the strengthened junctions, from $F_{max} = 45$ pN for the wild-type EC to 74 pN for $E_{para} = 3150$ Pa, and further to 90 pN for $E_{para} = 4200$ Pa. For both cases of elevated E_{para}, the resistance of paracellular transmigration now surpasses that of the transcellular route. Thus, the model reproduces the observations of Martinelli *et al.* [3] that stiffening the EC near cell junctions can make the transcellular route preferable. Our mechanical tests have tentatively confirmed the hypothesis of tenertaxis.

4 Conclusion

As part of the immune reaction, leukocytes transmigrate across the endothelium either directly through the body of an endothelial cell (EC) (transcellular route) or through the junction between adjacent ECs (paracellular route). To rationalize the preference between the two routes, Martinelli *et al.* [3] hypothesized that leukocytes seek the path of least mechanical resistance in a process called tenertaxis. In this study, we have examined this hypothesis using numerical computation of the mechanical resistance encountered by the leukocyte protrusion during paracellular or transcellular penetration. Model predictions show that normally the paracellular route is the preferred route for human lung endothelia. Using model parameters corresponding to the human lung microvasculature, our computations show that the required force to penetrate the endothelium in the transcellular route ($F_{max} = 72$ pN) is greater than that of the paracellular route ($F_{max} = 45$ pN). This rationalizes the preference of leukocytes to use the paracellular route most of the time.

Motivated by experiments that enhanced the junctional integrity of endothelium through the use of modifying agents, we have demonstrated that by increasing the elastic modulus of the EC near the junction, the mechanical resistance of the paracellular route may surpass that of the transcellular route. This will make the transcellular route preferable, in agreement with experimental observations [3]. Thus, our mechanical tests have tentatively confirmed the hypothesis of tenertaxis.

Our model is purely mechanical, and aims at testing the mechanical feasibility of the tenertaxis hypothesis. Thus, it has incorporated many assumptions and simplifications. First, we have ignored all biochemical signaling in the complex process of diapedesis. In particular, we have neglected the kinetics of F-actin polymerization, which determines the force generation inside the invadosome-like protrusion (ILP), and the breakage of molecular bonds in the EC junction during paracellar transmigration. A more complete model should integrate such biochemical kinetics with the mechanical deformation of the EC. Second, our model does not account for the leukocyte nucleus. Instead, we follow the experimental work [2–4] in focusing solely on the ILP as the "probe" for measuring the resistance of various endothelial components. Because of the complex morphology and dynamic behavior of the leukocyte nucleus, its role in diapedesis is an open and actively debated question [37, 38]. Third, we model the EC as hyperelastic, and disregard the cytoplasm and potential viscoelastic responses of the endothelium [39]. Finally, we have treated the ILP as an

inert solid object. Experimental evidence suggests that there is a dynamic interaction between the leukocyte and the ECs. Through mechanical and chemical signaling pathways, the leukocyte may induce cortical contraction inside the EC to open up the cell junctions and facilitate paracellular passage [40, 41]. In return, the EC appears to modulate the lifetime of the ILP through an active feedback mechanism, such that unsuccessful protrusions retract quickly while more successful ones grow and persist much longer [33]. Thus, it is clear that leukocyte diapedesis is a complex process that involves a rich array of biochemical and mechanical processes. Tenertaxis is a simple but promising idea that explains the outcome from predominantly mechanical factors. Our modeling offers quantitative support for this concept.

We end by noting the clinical relevance of the above discussion. Endothelial barrier function is perturbed in many disease states (e.g. sepsis, COVID-19 and atherosclerosis, to name a few) that involve endothelial activation and enhanced leukocyte transit through the paracellular space. Once in the tissue, the leukocytes activate and promote inflammation and cause organ damage. The use of glucocorticoids, which "stiffen" the endothelial cell junctions by enhancing synthesis of junction proteins such as occludin and VE-cadherin, reduces leukocyte entry and dampens inflammation [42]. Endothelial barrier function is thus an important target of therapeutic discoveries for many inflammatory conditions.

Acknowledgement: The authors acknowledge financial support by the Natural Sciences and Engineering Research Council of Canada (Discovery Grant No. 2019-04162), MITACS (Accelerate Program) and by the Providence Airway Centre at the Centre for Heart Lung Innovation, St. Paul's Hospital. The computations were carried out at WestGrid (www.westgrid.ca) and Compute Canada (www.computecanada.ca), with software licensing through CMC Microsystems (www.cmc.ca). The authors would like to thank Mohamad Ali Bijarchi for help with software setup, and Mattia Bacca, Gwynn Elfring, Boris Stoeber and Edmond Young for comments and discussions.

References

[1] V. Kumar, A. K. Abbas, N. Fausto, J. C. Aster, Robbins and Cotran Pathologic Basis of Disease, 9th Edition, Elsevier Health Sciences, 2014.

[2] C. V. Carman, Mechanisms for transcellular diapedesis: probing and pathfinding by 'invadosome-like protrusions', J. Cell Sci. 122 (17) (2009) 3025–3035.

[3] R. Martinelli, A. S. Zeiger, M. Whitfield, T. E. Sciuto, A. Dvorak, K. J. Van Vliet, J. Greenwood, C. V. Carman, Probing the biomechanical contribution of the endothelium to lymphocyte migration: diapedesis by the path of least resistance, J. Cell Sci. 127 (17) (2014) 3720–3734.

[4] C. V. Carman, P. T. Sage, T. E. Sciuto, A. Miguel, R. S. Geha, H. D. Ochs, H. F. Dvorak, A. M. Dvorak, T. A. Springer, Transcellular diapedesis is initiated by invasive podosomes, Immunity 26 (6) (2007) 784–797.

[5] C. Lim, E. Zhou, S. Quek, Mechanical models for living cells – a review, J. Biomech. 39 (2) (2006) 195–216.

[6] G. I. Bell, M. Dembo, P. Bongrand, Cell adhesion. competition between nonspecific repulsion and specific bonding., Biophys. J. 45 (6) (1984) 1051.

[7] L. A. Chtcheglova, L. Wildling, J. Waschke, D. Drenckhahn, P. Hinterdorfer, AFM functional imaging on vascular endothelial cells, J. Mol. Recognit. 23 (6) (2010) 589–596.

[8] E. Dejana, Endothelial cell–cell junctions: happy together, Nat. Rev. Mol. Cell Biol. 5 (2004) 261–270.

[9] M. Dembo, D. Torney, K. Saxman, D. Hammer, The reaction-limited kinetics of membrane-to-surface adhesion and detachment, Proc. R. Soc. London, Ser. B 234 (1274) (1988) 55–83.

[10] Q. Jin, C. Verdier, P. Singh, N. Aubry, R. Chotard-Ghodsnia, A. Duperray, Migration and deformation of leukocytes in pressure driven flows, Mech. Res. Commun. 34 (5) (2007) 411–422.

[11] B. Garipcan, S. Maenz, T. Pham, U. Settmacher, K. D. Jandt, J. Zanow, J. Bossert, Image analysis of endothelial microstructure and endothelial cell dimensions of human arteries–a preliminary study, Adv. Eng. Mater. 13 (1-2) (2011) B54–B57.

[12] M. Sato, K. Nagayama, N. Kataoka, M. Sasaki, K. Hane, Local mechanical properties measured by atomic force microscopy for cultured bovine endothelial cells exposed to shear stress, J. Biomech. 33 (1) (2000) 127–135.

[13] A. L. James, P. S. Maxwell, G. Pearce-Pinto, J. G. Elliot, N. G. Carroll, The relationship of reticular basement membrane thickness to airway wall remodeling in asthma, Am. J. Respir. Crit. Care Med. 166 (12) (2002) 1590–1595.

[14] J. Escribano, M. B. Chen, E. Moeendarbary, X. Cao, V. Shenoy, J. M. Garcia-Aznar, R. D. Kamm, F. Spill, Balance of mechanical forces drives endothelial gap formation and may facilitate cancer and immune-cell extravasation, PLoS Comput. Biol. 15 (5) (2019) e1006395.

[15] U. Moran, R. Phillips, R. Milo, Snapshot: key numbers in biology, Cell 141 (7) (2010) 1262–1262.

[16] H. Wolburg, K. Wolburg-Buchholz, B. Engelhardt, Diapedesis of mononuclear cells across cerebral venules during experimental autoimmune encephalomyelitis leaves tight junctions intact, Acta Neuropathol. 109 (2) (2005) 181–190.

[17] X. Cao, E. Moeendarbary, P. Isermann, P. Davidson, X. Wang, M. Chen, A. Burkart, J. Lammerding, R. Kamm, V. Shenoy, A chemomechanical model for nuclear morphology and stresses during cell transendothelial migration, Biophys. J. 111 (7) (2016) 1541 – 1552.

[18] P. Wriggers, Computational Contact Mechanics, Springer-Verlag Berlin Heidelberg, 2006.

[19] H. Ladjal, J.-L. Hanus, A. Pillarisetti, C. Keefer, A. Ferreira, J. P. Desai, Atomic force microscopy-based single-cell indentation: Experimentation and finite element simulation, in: 2009 IEEE/RSJ International Conference on Intelligent Robots and Systems, IEEE, 2009, pp. 1326–1332.

[20] P. Viswanathan, Y. Ephstein, J. G. Garcia, M. Cho, S. Dudek, Differential elastic responses to barrier-altering agonists in two types of human lung endothelium, Biochem. Biophys. Res. Commun. 478 (2) (2016) 599–605.

[21] L. Isac, G. Thoelking, A. Schwab, H. Oberleithner, C. Riethmuller, Endothelial F-actin depolymerization enables leukocyte transmigration, Anal. Bioanal. Chem. 399 (7) (2011) 2351–2358.

[22] P. Panorchan, J. P. George, D. Wirtz, Probing intercellular interactions between vascular endothelial cadherin pairs at single-molecule resolution and in living cells, J. Mol. Biol. 358 (3) (2006) 665–674.

[23] Z. Liu, J. L. Tan, D. M. Cohen, M. T. Yang, N. J. Sniadecki, S. A. Ruiz, C. M. Nelson, C. S. Chen, Mechanical tugging force regulates the size of cell–cell junctions, PNAS 107 (22) (2010) 9944–9949.

[24] A. B. Mathur, G. A. Truskey, W. M. Reichert, Atomic force and total internal reflection fluorescence microscopy for the study of force transmission in endothelial cells, Biophys. J. 78 (4) (2000) 1725–1735.

[25] A. B. Mathur, A. M. Collinsworth, W. M. Reichert, W. E. Kraus, G. A. Truskey, Endothelial, cardiac muscle and skeletal muscle exhibit different viscous and elastic properties as determined by atomic force microscopy, J. Biomech. 34 (12) (2001) 1545–1553.

[26] D. Zeng, T. Juzkiw, A. T. Read, D. W.-H. Chan, M. R. Glucksberg, C. R. Ethier, M. Johnson, Young's modulus of elasticity of Schlemm's canal endothelial cells, Biomech. Model. Mechanobiol. 9 (1) (2010) 19–33.

[27] K. D. Costa, A. J. Sim, F. C. Yin, Non-Hertzian approach to analyzing mechanical properties of endothelial cells probed by atomic force microscopy, J. Biomech. Eng. 128 (2) (2006) 176–184.

[28] S. Barzilai, S. K. Yadav, S. Morrell, F. Roncato, E. Klein, L. Stoler-Barak, O. Golani, S. W. Feigelson, A. Zemel, S. Nourshargh, et al., Leukocytes breach endothelial barriers by insertion of nuclear lobes and disassembly of endothelial actin filaments, Cell Rep. 18 (3) (2017) 685–699.

[29] A. Labernadie, A. Bouissou, P. Delobelle, S. Balor, R. Voituriez, A. Proag, I. Fourquaux, C. Thibault, C. Vieu, R. Poincloux, G. M. Charrire, I. Maridonneau-Parini, Protrusion force microscopy reveals oscillatory force generation and mechanosensing activity of human macrophage podosomes, Nat. Commun. 5 (1) (2014) 5343.

[30] M. J. Footer, J. W. Kerssemakers, J. A. Theriot, M. Dogterom, Direct measurement of force generation by actin filament polymerization using an optical trap, PNAS 104 (7) (2007) 2181–2186.

[31] S. Dmitrieff, F. Nédélec, Amplification of actin polymerization forces, J. Cell Biol. 212 (7) (2016) 763–766.

[32] A. Mogilner, B. Rubinstein, The physics of filopodial protrusion, Biophys. J. 89 (2) (2005) 782–795.

[33] Y.-T. Yeh, R. Serrano, J. Fran*c*cois, J.-J. Chiu, Y.-S. J. Li, J. C. Del Álamo, S. Chien, J. C. Lasheras, Three-dimensional forces exerted by leukocytes and vascular endothelial cells dynamically facilitate diapedesis, PNAS 115 (1) (2018) 133–138.

[34] C. V. Carman, R. Martinelli, T lymphocyte–endothelial interactions: emerging understanding of trafficking and antigen-specific immunity, Front. Immunol. 6 (2015) 603.

[35] F. T. Arce, B. Meckes, S. M. Camp, J. G. Garcia, S. M. Dudek, R. Lal, Heterogeneous elastic response of human lung microvascular endothelial cells to barrier modulating stimuli, Nanomed. Nanotechnol. Biol. Med. 9 (7) (2013) 875–884.

[36] J. G. Garcia, F. Liu, A. D. Verin, A. Birukova, M. A. Dechert, W. T. Gerthoffer, J. R. Bamberg, D. English, Sphingosine 1-phosphate promotes endothelial cell barrier integrity by edg-dependent cytoskeletal rearrangement, J. Clin. Invest. 108 (5) (2001) 689–701.

[37] H. R. Manley, M. C. Keightley, G. J. Lieschke, The neutrophil nucleus: An important influence on neutrophil migration and function, Front. Immunol. 9 (2018) 2867.

[38] F. M. Marelli-Berg, S. Nadkarni, Displacing, squeezing, and ramming: The role of nuclear lamins in leukocyte migration, J. Leukoc. Biol. 104 (2) (2018) 235–236.

[39] G. Silvani, V. Romanov, C. D. Cox, B. Martinac, Biomechanical characterization of endothelial cells exposed to shear stress using acoustic force spectroscopy, Front. Bioeng. Biotechnol. 9 (2021) 21.

[40] N. Reymond, B. B. d'Água, A. J. Ridley, Crossing the endothelial barrier during metastasis, Nat. Rev. Cancer 13 (2013) 858–870.

[41] T. Russo, D. Stoll, H. Nader, J. Dreyfuss, Mechanical stretch implications for vascular endothelial cells: Altered extracellular matrix synthesis and remodeling in pathological conditions, Life Sci. 213 (2018) 214 – 225.

[42] E. Salvador, S. Shityakov, C. Förster, Glucocorticoids and endothelial cell barrier function, Cell Tissue Res. 355 (3) (2014) 597–605.

Supporting Information for "A mechanical test of the tenertaxis hypothesis for leukocyte diapedesis"

S.M. Amin Arefi[1], Cheng Wei Tony Yang[2], Don D. Sin[2] and James J. Feng[1,3*]

[1] Department of Chemical and Biological Engineering, University of British Columbia, Vancouver, BC V6T 1Z3, Canada

[2] Centre for Heart Lung Innovation, St Paul's Hospital and University of British Columbia, Vancouver, BC V5Z 1M9, Canada

[3] Department of Mathematics, University of British Columbia, Vancouver, BC V6T 1Z2, Canada

(April 12, 2021)

1 Numerical techniques

We used COMSOL Multiphysics to solve the system of governing equations. The simulations consist in solving for the elastic deformation of the endothelial cells (ECs) and the basement membrane as the invadosome-like protrusion (ILP) penetrates into the ECs or the junctional gap under prescribed displacement or force.

Typical finite-element meshes are shown in Fig. S1. For the paracellular simulations, we used a grid with about 360,000 tetrahedral elements. Note the refinement in the junctional gap to ensure adequate spatial resolution (Fig. S1a). The ILP is essentially rigid. But it turned out to be more convenient to model it as elastic in the COMSOL module. Thus, we have meshed it as a circular cylinder with a hemispherical end, with a very high elastic modulus $E = 205$ GPa.

For the transcellular simulations, we typically deployed about 12000 quad and triangular elements. To capture the very large strain in the transcellular setup, we utilized very high aspect-ratio elements (Fig. S1b) with quintic Lagrange shape function near the site of protrusion. These elements appear as highly elongated rectangles in the region below the tip of the ILP. As the ILP compresses this region, the elements eventually take on more moderate aspect ratios toward the later stage of the simulation.

We have done numerical experimentation to check the convergence of the results with respect to spatial resolutions, and the meshes shown in Fig. S1 turned out to be sufficient. With a coarse mesh of about 140,000 elements, for example, the paracellular simulation predicted a resistance

*Corresponding author. E-mail: james.feng@ubc.ca

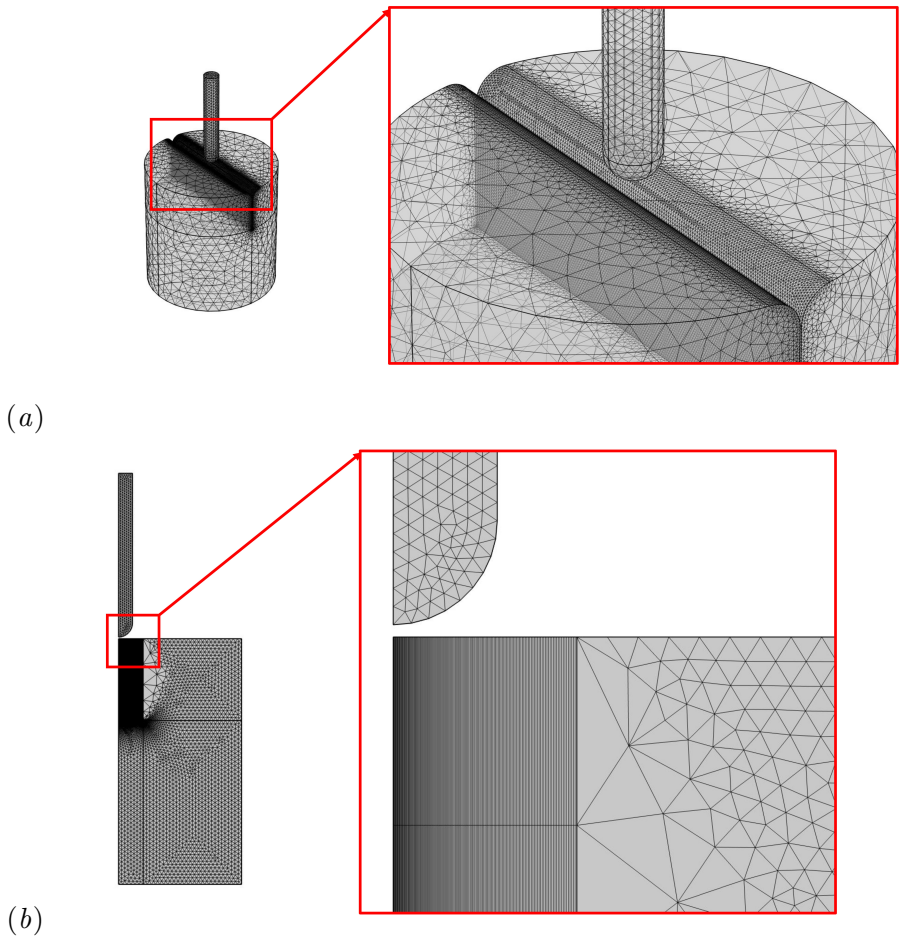

Figure S1: Grids used for computing the penetration of the leukocyte protrusion into the EC through (a) the paracellular route and (b) the transcellular route. Note the highly elongated initial mesh in the region below the rod in (b).

force within 1.8% of that of the finer mesh of 360,000 elements. Besides, we found a maximum time step of $\Delta t = 0.001$ s to be adequate for resolving the transients in the dynamic simulations.

2 Parametric study

For the simulation results presented in the main paper, we have used the baseline parameters that tabulated in Table 1. Moreover, we have carried out parametric studies to investigate how the mechanical resistance depends on the key parameters, including the undeformed gap size between two adjacent ECs, the spring constant of VE-cadherin bonds, the diameter of the ILP, and the elastic modulus for transcellular protrusion.

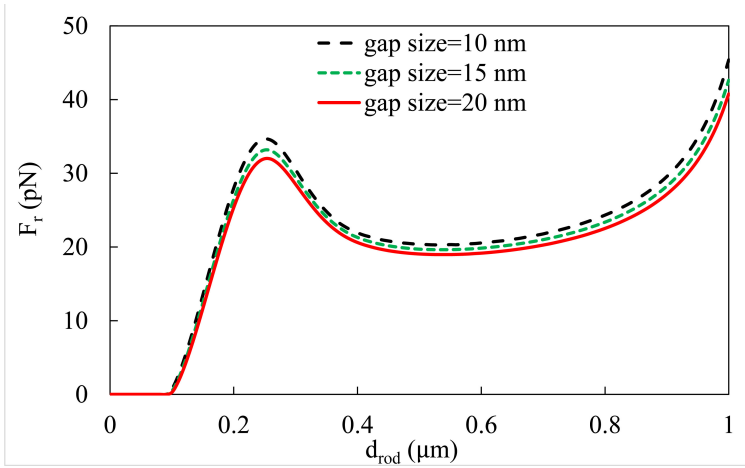

Figure S2: Effect of the EC junctional gap size on the resistance force during paracellular protrusion.

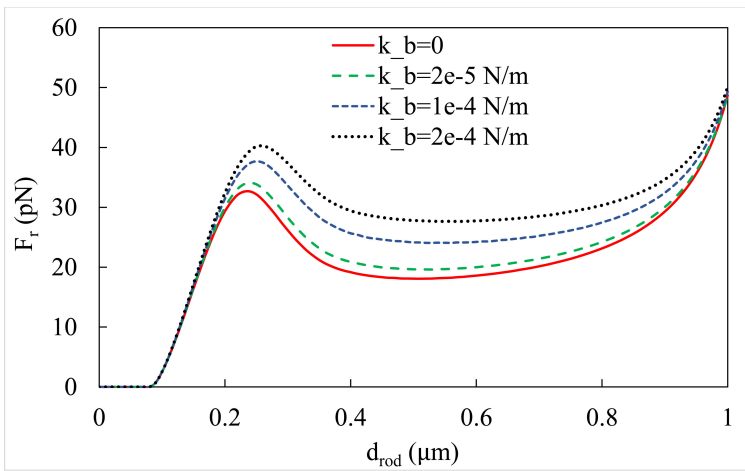

Figure S3: Effect of the spring constant k_b of the VE-cadherin bonds on the resistance force during paracellular protrusion.

2.1 Effect of the undeformed junctional gap size

Figure S2 depicts the effect of undeformed gap size on the resistance force during paracellular protrusion. As the gap size d_{gap} increases from the baseline of 10 nm to 20 nm, a reasonable range based on experimental data [1], the resistance force decreases only slightly. As the diameter of the ILP is 340 nm, much wider than the gap size, the paracellular protrusion entails a great elastic deformation on the EC next to the gap. The range of d_{gap}, therefore, corresponds to a relatively small percentage change in the amount of elastic strain in the ECs.

2.2 Effect of the spring constant of VE-cadherin bonds

Figure S3 shows the effect of stiffness of the VE-cadherin bonds on the resistance force of paracellular protrusion. The key observation is that although the first peak of the resistance force increases with increase in k_b, the maximum resistance force at the breakthrough is a very weak function of

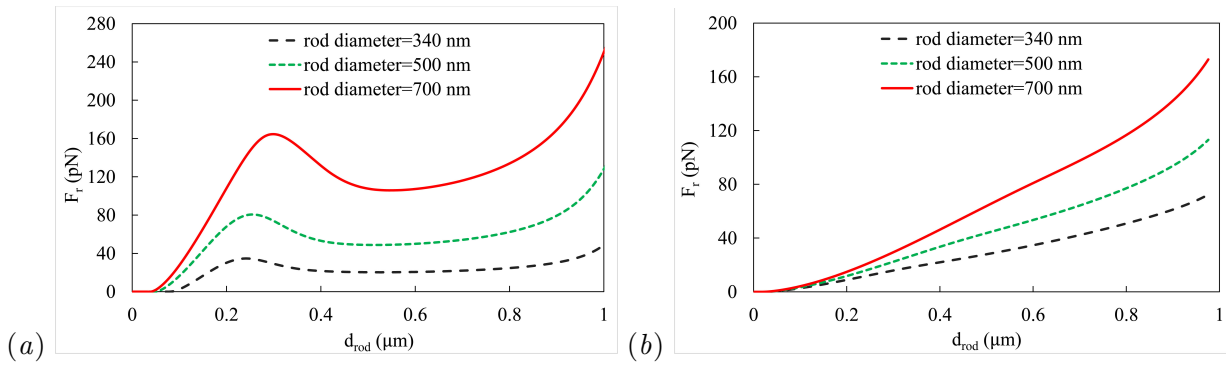

Figure S4: Effect of the rod diameter in resistance force in (a) the paracellular setup and (b) the transcellular setup.

the spring constant. Even if we eliminate these bonds altogether ($k_b = 0$), the maximum resistance force decreases by less than 0.1%. As discussed in the main text, this is because the bond force is aligned across the gap, perpendicular to the direction of the ILP protrusion. Thus, its effect is felt by the ILP only indirectly through modifying the EC surface shape. This explains why the relative sensitivity at the first peak of F_r, when the apical part of the gap is opened, and the lack thereof toward the breakthrough at the end, when the gap is mostly expanded uniformly.

2.3 Effects of the diameter of the leukocyte protrusion

Experimental observations have suggested a range for the diameter of the protruding ILP (or "the rod") as between 200 nm and 1 μm [2,3], and we have chosen 340 nm as our baseline value. To see the effect of protrusions thickness on the mechanical resistance, we have increased the diameter of the rod in our paracellular and transcellular simulations (Fig. S4). As can be expected, a thicker rod requires a larger force for the successful protrusion in both the paracellular and transcellular routes. Although this variability changes the magnitude of the forces, it probably would not qualitatively affect the comparison between the two routes or modify the tenertaxis argument.

2.4 Effect of the endothelial elastic modulus on transecllular protrusion

As mentioned in the main paper, the leukocyte protrusion is known to induce local remodeling of the EC cortex and softening of the local modulus [4]. The maximum softening is estimated to be about 10 folds during transcellular penetration. In this section, we vary the degree of this softening and examine its effect on the resistance of the transcellular route. Thus, the EC modulus is raised from the baseline value of $E_{tran} = 180$ Pa to 360 Pa and 1800 Pa. Figure S5 plots the resistance force F_r during transcellular penetration for these three values of E_{trans}. The peak forces for the penetration to the EC body with $E_{tran} = 1800$ Pa is 635 pN, much higher than that of 72 pN predicted for the baseline modulus of $E_{tran} = 180$ Pa. Therefore, successful transcellular transmigration depends critically on the cortex disassembly and softening.

The stronger resistance at the elevated EC stiffness of $E_{tran} = 1800$ Pa can be appreciated in

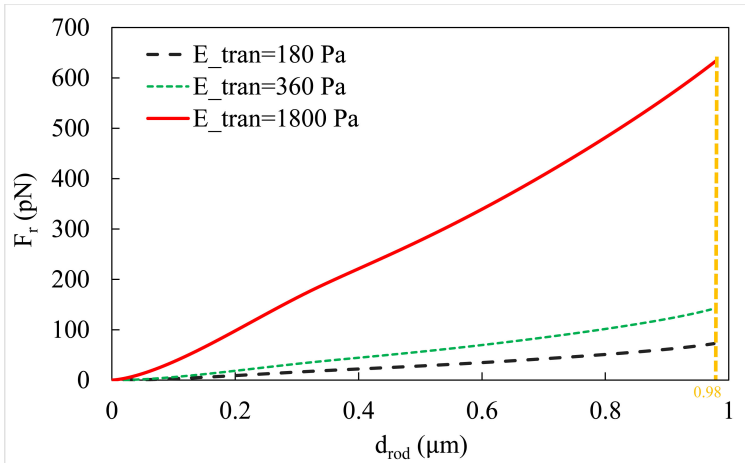

Figure S5: The effect of the endothelial modulus E_{tran} on the resistance force during transcellular penetration.

an experimental context. Ng *et al.* [5] used the tip of the cantilever in an atomic force microscope (AFM) to indent the cell body of human umbilical vein endothelial cells (HUVECs). Depending on the location, to produce a transcellular tunnel about 2 μm in diameter required a force between 5 and 100 nN. Hence, the normal stress for the formation of this tunnel was between 1600 and 31800 Pa. In our model predictions, the average normal stress required to penetrate the cell body for E_{tran}=1800 Pa is about 7000 Pa, which is within the experimental range of Ng *et al.* [5]. Obviously, their AFM cantilever does not induce EC cortical remodeling as an attached leukocyte would [4]. Thus, a much greater force or pressure is needed on the AFM cantilever to produce the transcellular tunnel than the protrusive force required of a leukocyte *in vivo*.

3 Dynamic simulation

Most of the results in the main paper are based on quasi-static calculations of the resistance force on the ILP that penetrates into the EC junction or the cell body with prescribed movement. To demonstrate that such results are relevant to the dynamic process of ILP protrusion driven by a constant force, we have carried out such dynamic simulations as well.

We applied a constant driving force of $F_d = 100$ pN on the ILP rod, which exceeds the maximum resistance expected from the quasi-static calculations. In the paracellular route, the EC resistance peaks when the tip of the rod reaches about 1/4 of the EC thickness (see Figs. S2 and S3, and Fig. 3 of the main paper). Afterwards, we anticipate an abrupt acceleration of the rod as the resistance drops with penetration depth. Such a sudden movement causes problems with the dynamic time-stepping of the simulation, especially because the very small mass of the ILP (estimated at $m_{rod} = 1.6 \times 10^{-12}$ g). To avoid this difficulty, we have added a damping force on the rod: $F_d = k_d v_{rod}$, where v_{rod} is the instantaneous velocity of the rod, and $k_d = 10^{-4}$ N·s/m is a damping coefficient. Under the driving force, the EC resistance and the damping force, the rod moves according to Newton's second law. The process is shown in Movie 2.

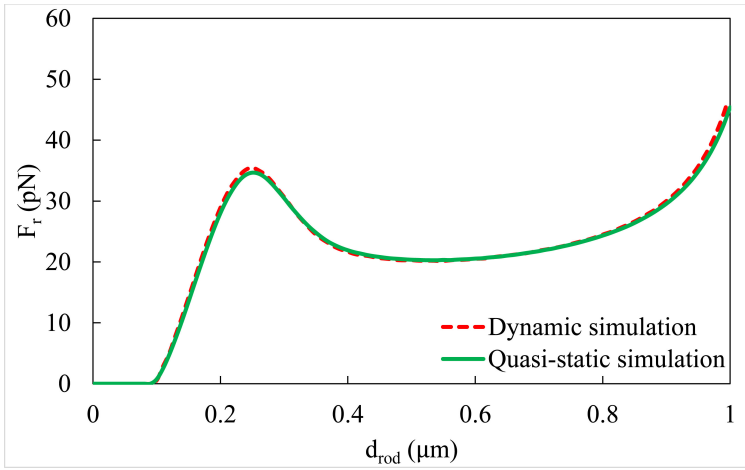

Figure S6: Contact resistance force by the endothelial cells during paracellular penetration: comparison between the dynamic simulation and the quasi-static calculation. The former tracks the movement of the ILP under a constant driving force $F_d = 100$ pN, whereas the latter prescribes the displacement of the ILP.

For a more quantitative comparison between the quasi-static and dynamic calculations, we have backed out the EC resistance force F_r from the equation of motion for the ILP in the dynamic simulation, and plotted it together with the resistance force previously computed from the quasi-static problem (Fig. 3 of the main paper). Figure S6 shows that the quasi-static and dynamic results practically coincide with each other. This support our claim in the main paper for the validity of the quasi-static protocol in calculating the EC resistance.

4 Supplemental movies

Three supplemental movies can be downloaded from the article's home page. Below are their captions.

Movie 1: Animation of the quasi-static paracellular protrusion. The color contours indicate von-Mises stress in Pa. The downward movement of the rod is prescribed with a step size of 10 nm. The numbers on the upper left corner indicate, in micron, the displacement of the tip of the rod from its initial position, which is 10 nm above the flat portion of the EC apical surface. Thus, the displacement is 1.01 μm on the final frame when the tip reaches the breakthrough depth of d_b =1 μm.

Movie 2: Animation of the dynamic simulation of paracellular protrusion driven by a constant driving force of 100 pN on the rod. The color contours indicate von Mises stress in Pa. To represent the ILP as a nearly rigid rod, we have assigned a very high modulus (205 GPa) to it, and the stress inside the rod reflects the driving force applied on its upper end and its contact with the ECs at the tip.

Movie 3: Animation of the quasi-static transcellular protrusion. The color contours indicate von Mises stress in Pa. The downward movement of the rod is prescribed with a step size of 5 nm.

References

[1] G. I. Bell, M. Dembo, P. Bongrand, Cell adhesion. competition between nonspecific repulsion and specific bonding., Biophysical journal 45 (6) (1984) 1051.

[2] C. V. Carman, P. T. Sage, T. E. Sciuto, A. Miguel, R. S. Geha, H. D. Ochs, H. F. Dvorak, A. M. Dvorak, T. A. Springer, Transcellular diapedesis is initiated by invasive podosomes, Immunity 26 (6) (2007) 784–797.

[3] C. V. Carman, Mechanisms for transcellular diapedesis: probing and pathfinding by 'invadosome-like protrusions', J. Cell Sci. 122 (17) (2009) 3025–3035.

[4] L. Isac, G. Thoelking, A. Schwab, H. Oberleithner, C. Riethmuller, Endothelial F-actin depolymerization enables leukocyte transmigration, Anal. Bioanal. Chem. 399 (7) (2011) 2351–2358.

[5] W. P. Ng, K. D. Webster, C. Stefani, E. M. Schmid, E. Lemichez, P. Bassereau, D. A. Fletcher, Force-induced transcellular tunnel formation in endothelial cells, Molecular biology of the cell 28 (20) (2017) 2650–2660.